










THz optical beat-note detection with a fast superconducting hot electron bolometer operating up to 31 GHz

G. TORRIOLI,¹ A. FORRER,²  M. BECK,² P. CARELLI,¹
F. CHIARELLO,¹ J. FAIST,²  A. GAGGERO,¹  E. GIOVINE,¹
F. MARTINI,¹  U. SENICA,²  R. LEONI,¹ G. SCALARI,²  AND S.
CIBELLA^{1,*} 

¹*Istituto di Fotonica e Nanotecnologie, Via Del Fosso del Cavaliere 100, 00133 Roma, Italy*

²*Institute for Quantum Electronics, Department of Physics, ETH Zürich, 8093 Zürich, Switzerland*

**sara.cibella@ifn.cnr.it*

Abstract: We study the performance of a hot-electron bolometer (HEB) operating at THz frequencies based on superconducting niobium nitride films. We report on the voltage response of the detector over a large electrical detection bandwidth carried out with different THz sources. We show that the impulse response of the fully packaged HEB at 7.5 K has a 3 dB cutoff around 2 GHz. Remarkably, detection capability is still observed above 30 GHz in an heterodyne beating experiment using a THz quantum cascade laser frequency comb. Additionally, the HEB sensitivity has been evaluated and an optical noise equivalent power NEP of 0.8 pW/ \sqrt{Hz} has been measured at 1 MHz.

© 2023 Optica Publishing Group under the terms of the [Optica Open Access Publishing Agreement](#)

1. Introduction

Hot Electron Bolometers (HEBs) are extremely sensitive detectors at frequencies above 1 THz and they are vastly employed in astronomical observations to map THz lines with a very high spectral resolution [1]. At the same time such devices present an intrinsically wide electrical bandwidth, making them appealing for applications in the THz range where the quest for high-speed detectors [2] is boosted by renewed interest in the field of ultrafast THz physics [3] and in the new studies of frequency comb technology [4,5]. For example, a new spectroscopic technique has been recently developed to demonstrate that all modes in the spectrum of a comb are uniformly spaced and phase coherent (i.e., SWIFT spectroscopy, Shifted Wave Interference Fourier Transform Spectroscopy) [6]. Such measurement relies on a fast detector capable to detect the optical beat notes, typically lying in the 1-30 GHz regime. We investigate the performance of our detector in this scenario of high power THz sources [7] and extremely fast signals. Superconducting hot electron bolometers are considered an excellent technological solution because of their extreme sensitivity and response beyond tens of GHz [8]. The great advantage of this bolometer, made of an ultrathin layer of NbN film, is that it combines a small heat capacity with high heat conductivity resulting in a time constant down to 40 ps for small optimized devices [8]. Furthermore, compared to competing technologies like superconductor-insulator-superconductor tunnel junctions and Schottky diodes, the HEB, as a pure thermal detector, does not possess any intrinsic energy scale limitation of the detection mechanism [9] and, it is useful throughout the IR and THz spectral regions [10,11].

With respect to the cooling mechanism of electrons, HEBs are divided into phonon-cooled and diffusion-cooled, depending on where the excess energy of the electrons are primarily removed, through substrate or through contacts, respectively [12].

Here we propose a phonon-cooled hot-electron bolometer coupled to a logarithmic spiral antenna [13] embedded in a coplanar waveguide (CPW) that allows a packaging with a microwave

end-launch connector. The aim of this paper is to demonstrate experimentally the high-speed operation of fabricated HEB using impulse response measurements [14]; short (ps), broadband THz pulses emitted using a compact, commercial terahertz time-domain spectrometer as well as higher intensity signal produced by a quantum cascade THz laser frequency comb, are employed. The frequency response of the bolometer has been characterized using a wide bandwidth (>30 GHz) RF spectrum analyzer. Furthermore, we provide a full characterization of our device on the basis of a hot electron model.

2. HEB fabrication and experimental setup

The HEB consists of a 1 μm -wide, 300 nm long and 6 nm thick NbN strip (bridge), fabricated on a highly resistive Si substrate (see Fig. 1(c)). The superconducting layer has been deposited by means of a reactive dc magnetron sputtering in Ar/N₂ gas mixture at 750 °C [10]. The bridge is connected to a self-complementary spiral antenna made of a 180 nm thick Ti/Au bilayer, embedded in a coplanar waveguide (with an impedance of ~ 50 Ohm). The inner diameter of the antenna is 7 μm . Starting from a silicon wafer coated with the NbN film, the HEB fabrication process uses the high resolution and realignment capability of a direct-writing electron beam lithography (EBL). In the first step, the Ti/Au layer is deposited on top of a PMMA resist mask, from which spiral antenna, wiring, contact pads and alignment marks are obtained by lift-off. In the second step, we define the HEB bridge by using a mask of hydrogen silsequioxane (HSQ) resist and successively etching away the unprotected NbN film by reactive ion etching. In Fig. 1(a) and (b) a SEM micrograph of the device fabricated is shown.

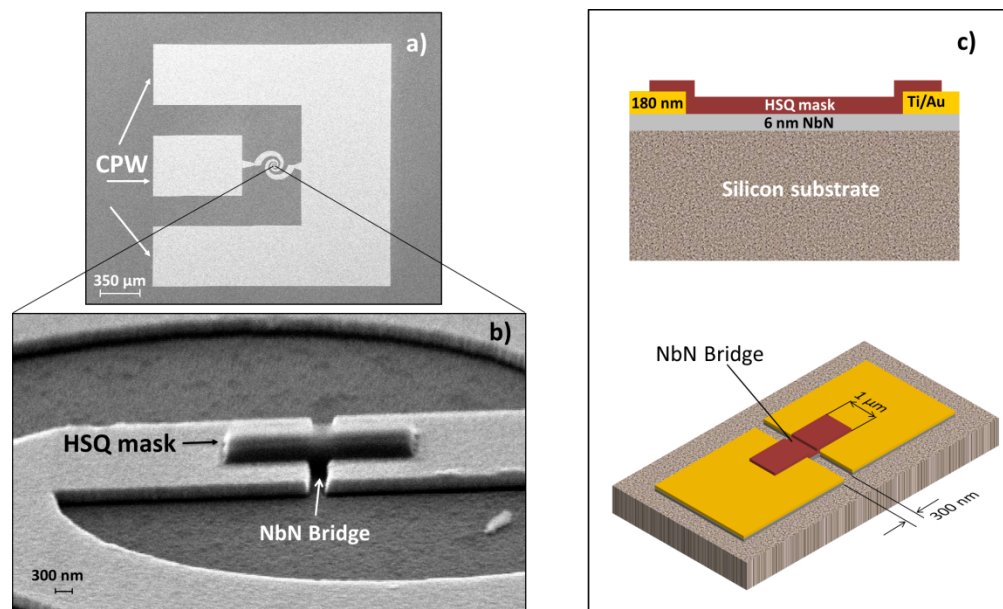


Fig. 1. SEM micrograph and sketch of the device fabricated: (a) SEM micrograph detail of the coplanar waveguide and the spiral antenna. (b) Zoom in of the bolometric element in the center of the spiral antenna showing the detail of the HSQ mask. (c) Sketch of the device showing the arrangement of the layers.

The radiation coupling to the antenna is further enhanced by tightly pressing a high-resistivity hyper-hemispherical Si lens, 6 mm in diameter, onto the silicon backside surface. The fabricated HEB, is mounted onto a copper holder in vacuum, screwed on the cold plate and cooled down by

using either: i) a helium flow cryostat for the heterodyne frequency measurements performed with the TDS (time-domain spectroscopy) system and the QCL source; ii) a pulse tube refrigerator for the voltage responsivity and NEP measurements. The optical windows of both cryostats are equipped with cold optical filters to suppress undesired wavelengths. In the setup utilized for the NEP measurements, we used a low noise cryogenic amplifier (LNA, CITLF1 by Cosmic Microwave Technology Inc. 40 dB gain, 0.001–1.5 GHz bandwidth and noise temperature ~ 9 K) connected by means of a bias-tee to our HEB. To calibrate the HEB at 1 MHz we use a homogeneous multimode THz quantum cascade laser operating at 3 THz central frequency [15].

3. Impulse and frequency response

The frequency response of the HEB is studied by using optical short pulses generated by a mode locked Erbium telecom fibre laser and a photoconductive antenna of a commercial, time domain THz spectrometer (TeraSmart, Menlo Systems), combined with a spectrum analyzer (SA) (see inset Fig. 2(d)). In this case a cold, FluoroGold low-pass filter is mounted on the radiation shield of the helium flow cryostat, to cut off the infrared background. The filter transmission spectrum is shown in Fig. 2(a).

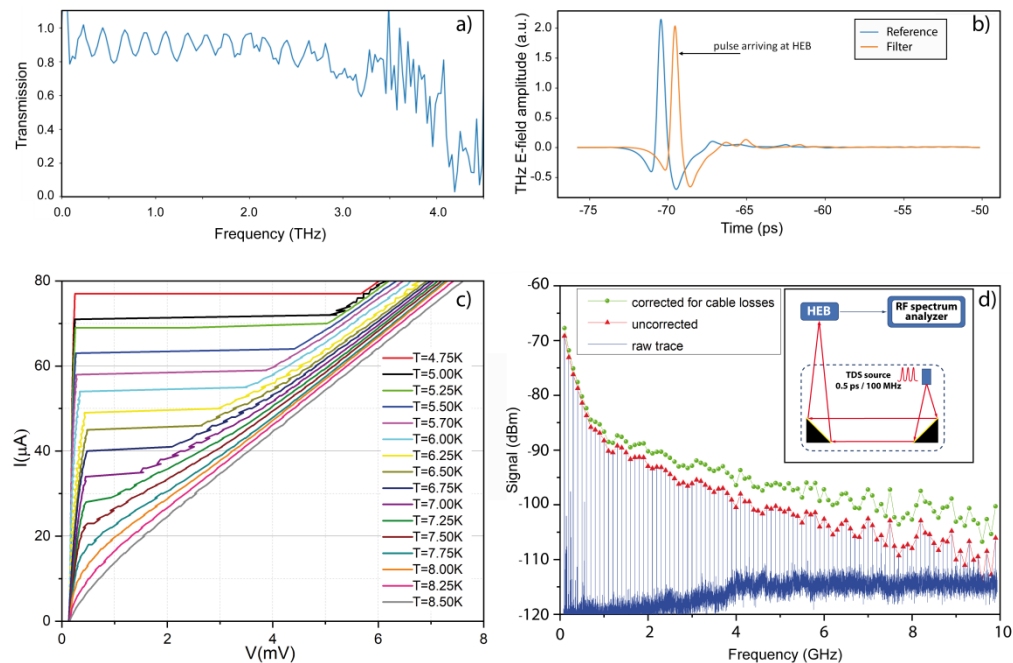


Fig. 2. (a) Transmission spectrum of of the FluoroGold filter used to block the incoming infrared radiation. (b) THz pulse arriving at HEB before and after the low pass filter used. (c) Experimental current-voltage (I-V) characteristics of the HEB taken in different heating conditions (TDS signal blanked). (d) Harmonics of the erbium laser beat-note up to 10 GHz biasing the HEB at 21 μ A at $T = 7.5$ K. Data are corrected including losses due to RF cable in the cryostat. ((d) inset) Experimental setup for measuring the impulse response of the HEB using THz picosecond pulses produced by a commercial photoconductive antenna illuminated by an Erbium-doped fiber mode-locked laser.

The THz pulse, induced by a femtosecond laser (<90 fs) with a repetition rate of 100 MHz, has a FWHM of about 0.5 ps and can be regarded as a good approximation of a delta-function pulse with respect to GHz frequencies. In Fig. 2(b) THz pulse arriving at HEB before and after

the FluoroGold filter is shown. For an ideally fast detector, i.e. flat frequency response, this THz signal would induce beating signals with nearly equal peak amplitudes within the GHz range we consider. Before going into the TDS results, we investigate the HEB I-V in the dark. Figure 2(c) shows the experimental I-V characteristics of the HEB, obtained with the TDS blanked but operating. We set the operating temperature for our measurements using a resistive heater and we took the family of I-V characteristics changing the bath temperature from 4.5 K to 8.5 K. The HEB fabricated has a normal state resistance (R_n) of 80 Ω and a critical current of 80 μA at 4.2 K without illumination from THz-TDS.

Now we unblock the optical path and measure for several temperatures and bias points the fundamental and the harmonic beating signals induced by the TDS system at frequencies (100, 200, 300, . . . , and so on up to 10000 MHz on the HEB with the SA). An example at 7.5 K biased at 21 μA is shown in Fig. 2(d). The blue curve shows the raw trace from the SA, the red triangle mark the peaks of each beating signal and the green dots represents the corrected peaks by subtracting the RF path losses up to the wire bonds of the HEB. Therefore, the green curve in Fig. 2(d), resembles to a good degree the intrinsic frequency response of the HEB. At frequencies above 10 GHz the residual path on the HEB chip should be further optimized since the RF wavelengths become shorter. The HEB is now biased at different currents of the I-V curves and its frequency response is measured as described before in the temperature range of 4.5-8 K. When the HEB is operated at temperatures far from the T_c , by increasing the bias current, the I-V curves show a sudden jump from the superconducting branch to the resistive branch. On the other hand when the HEB is operated in a temperature range close to the T_c , the I-V curve jump does not occur anymore: this corresponds to a stable hotspot in the HEB which will expand gradually with the bias until the whole film goes into normal state [16]. In this temperature range the HEB can be polarized in each point of the I-V characteristics as long as dV/dI is continuous avoiding noisy instabilities.

More in detail, we consider the behavior of the HEB at 7.5 K (see Fig. 3). We mark the different bias points along the I-V with different colors (Fig. 3(a)). We first normalize all response curves to the maximum amplitude for all traces (in this case at 20 μA , 100 MHz) highlighting the behavior of the detector responsivity. We experimented a dependence of the bandwidth with the bias point and a possible reason for this behavior is due to a dependence of the self-heating parameter. This parameter, which describes the effect of the electro-thermal feedback between the electron temperature and the DC bias supply, depends on bias points themselves and slightly modifies the HEB time constant [12,17]. The bias point set at 20 μA , i.e., the best in terms of responsivity, rolls off quite fast with frequency, while signal at 5 μA is nearly 30 dB lower with a wider 3 dB bandwidth (BW) (see Fig. 3(b)). One should note that the 20 μA bias point results in the highest gain at all measured frequencies despite the rapid frequency response drop. Then we normalize all intermode beating signals to the maximum for each curve which allows a better comparison of the 3 dB BW. It can be clearly observed, that at this temperature the -3 dB cutoff is around 2 GHz for lower detector responsivity and the largest band biasing the HEB at 5 μA . This bias point would be optimal in application which need a flat response over a large BW. Therefore, combining the two graphs in Fig. 3(b) and (c), we have all the information necessary to choose the optimal point where one would like to operate the HEB depending on the specific application.

The same measurement data shown in Fig. 3(b) at 7.5 K can be further visualized in a 3D color map as shown in Fig. 3(d). Here we did not normalize to the peak intensity to show the relatively high signal levels up to 67 dBm of the beating signals, i.e. > 50 dB SNR. The white dashed lines represent the -3 dB and -15 dB cut off frequency. Similar plots are presented for different temperatures in Supplement 1.

It is important to point out that the HEB is still sensitive above 10 GHz, but the THz signal produced by the photoconductive antenna is too low to be detected. To probe the ultimate frequency limit of the HEB we detect the intermodal optical beat note by an injection-locked

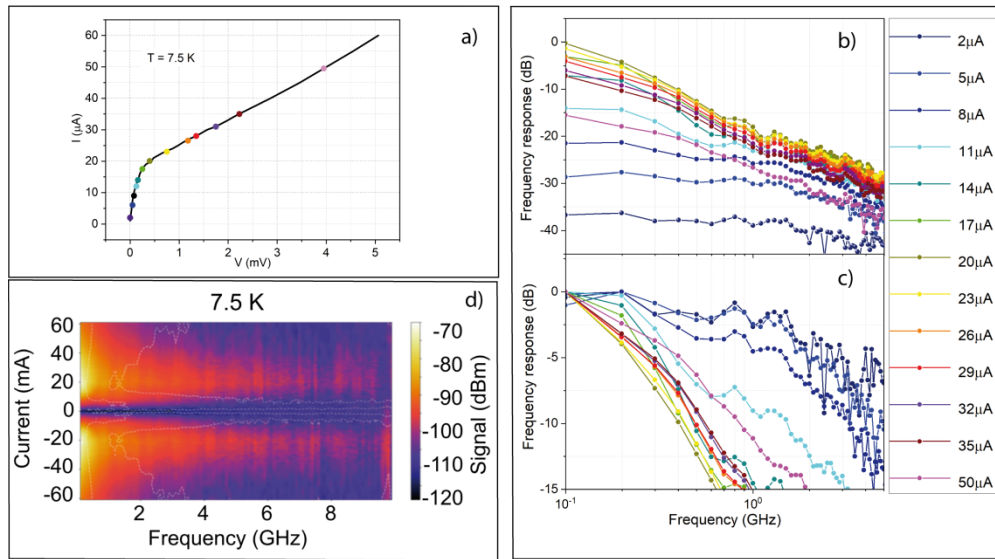


Fig. 3. Frequency response of the HEB at $T = 7.5$ K at the different bias conditions. (a) I-V curve at 7.5 K with colored different bias points. (b) All response curves are normalized to the maximum amplitude for all traces (in this case at 20 μ A, 100 MHz). (c) Normalizing all intermode beating signals to the maximum for each curve. (d) 3D color plot: the amplitude of the signal taken at different bias points vs the frequency response and the bias current. The dashed line shows the -3 dB and -15 dB cut off. Changing the bias point along the I-V curve, the -3 dB and -15 dB cut off change.

THz QCL frequency comb, centered around 2.6 THz (see spectrum in Fig. 4(a)), with emission powers in the lower mW range. This device has an optical mode spacing 10.5129 GHz. It should be noted that the QCL frequency comb is in a mixed state with both frequency and amplitude modulation and is therefore not producing discrete pulses such as a mode-locked laser, but rather a quasi-continuous periodic waveform. This is in contrast with the THz photoconductive source

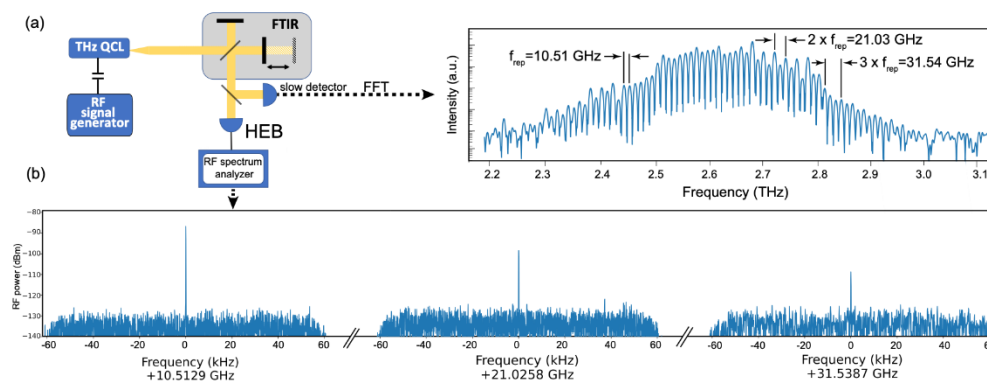


Fig. 4. (a) Experimental setup: an injection-locked THz QCL is coupled to a FTIR. The displayed spectrum corresponds to an 800 GHz bandwidth comb state with a repetition rate $f_{\text{rep}} = 10.15$ GHz. (b) Optical beat-notes detected with the HEB. Signals up to the third harmonic, corresponding to a frequency of $3 \times f_{\text{rep}} = 31.54$ GHz are detected with a SNR larger than 20 dB.

of the TDS system, which emits a train of 0.5 ps-long pulses with a repetition rate of 100 MHz. Therefore, the beating signals are expected to differ in peaks power and we cannot extract the frequency response from this measurement reliably. Nevertheless we are able to detect the optical beat-note of the laser up to its third harmonic (31.5387 GHz signal, see Fig. 4(b)), with a signal-to-noise ratio of 20 dB. It is important to note the analogy between Fig. 2(d) and Fig. 4(b), both showing the coherence of the combs even though in case of the THz QCL comb the electric field does not show pulses in the time-domain [5]. It is important as well to underline the fact that in the case of the THz QCL beat-note measurement no RF amplifier was employed because the signal extracted from the HEB cryostat was directly fed into the spectrum analyzer.

4. Device modeling

We used the two temperature (2 T) theoretical model [18,19] to describe the electro-heating process that occurs in a HEB. In this way, we can extract the response of the HEB alone from the rest of the circuit in order to understand the measurements described in the previous sections. This model works for non-equilibrium superconductors maintained at temperature T near the superconducting transition temperature T_c . The classic description of the HEB under operation is that the incoming radiation and the electrical bias heat up the electrons in the NbN and induce a local resistance [20,21]: an uniform enhancement of the electron temperature is assumed higher than the phonon-temperature. The response of the detector is controlled by the electron temperature, i.e., hot electrons, and by the local resistivity. Under operating conditions, the whole detector, including the contacts, is in the superconducting state, except for the centre of the NbN bridge, where the resistance emerges due to the increase in the electron temperature. If the modulation of the electron temperature can follow the modulation due to the incoming signal also the resistivity of the HEB will be modulated and consequently a voltage signal is measured. Following the 2 T model the superconducting NbN film can be described in terms of two coexisting subsystems: electrons and phonons. In case the temperature T is close to the critical temperature T_c , we can assume that the effective temperatures of the electron and phonon subsystems (T_e and T_{ph} , respectively) are instantly and uniformly reached. With this hypothesis the hot electron effect in superconductors can be described by [22]:

$$\frac{dT_e}{dt} = -\frac{T_e - T_{ph}}{\tau_{e-ph}} - \frac{T_e - T_b}{\tau_{diff}} + \frac{j^2 \rho(T_e, I_b) + p(t)}{c_e} \quad (1)$$

$$\frac{dT_{ph}}{dt} = \frac{c_e}{c_{ph}} \frac{T_e - T_{ph}}{\tau_{e-ph}} - \frac{T_{ph} - T_b}{\tau_{esc}} \quad (2)$$

where, T_b is the bath temperature, $\rho(T_e, I_b)$ is the local resistivity of the HEB in the normal state, j is the current density and $p(t)$ is the rf power absorbed per unit volume. The electron-phonon interaction time and phonon escape time are $\tau_{e-ph} = 500$ [ps K^{1.6}] $T_e^{-1.6}$ [16,22] and $\tau_{esc} = 10.9$ [ps nm] d , respectively. The film thickness is d , the diffusion coefficient in the NbN is $D = 0.45$ cm² s⁻¹, L the bridge length and $\tau_{diff} = L^2/(\pi^2 D)$ is the effective diffusion time constant. The electron and phonon specific heats are defined as $c_e = 1.85 \times 10^{-4}$ [J cm⁻³ K⁻²] T_e and $c_{ph} = 9.7 \times 10^{-6}$ [J cm⁻³ K⁻⁴] T_e^3 . In an HEB based on an ultra-thin NbN film deposited on a silicon substrate the relaxation times are typically $\tau_{e-ph} \approx 10$ -15 ps and $\tau_{esc} = 50$ ps $\ll \tau_{diff}$ (phonon cooling) [16]. To predict the current to voltage characteristics with the 2 T model, we start from the measured transition of the resistance (current-dependent) vs T of our HEB. Following the model proposed by Hajenius et al. [21] we approximated the $R(T)$ curve to a Fermi-Dirac-like (sigmoidal) function as introduced by Gershenson et al. [23,24]:

$$\frac{\rho(T_e)}{\rho_n} = \frac{1}{1 + e^{-(T_e - T_c)/\Delta T_c}} \quad (3)$$

which represents the local resistivity for a given local electron temperature T_e with ρ_n the resistivity in the normal state, T_c the critical temperature of our bolometer and ΔT_c the temperature transition width. The intrinsic transition is measured for different dc bias current. Figure 5(a) shows the experimental points (symbols) and the modelled curves (continuous curves).

Increasing the current, the $R(T, I_b)$ curves shifts to lower temperatures [20] and the downshift of the critical temperature T_c follows the equation

$$\frac{I_b}{I_c} = \left(1 - \frac{T_c(I_b)}{T_c(0)}\right)^{\gamma} \quad (4)$$

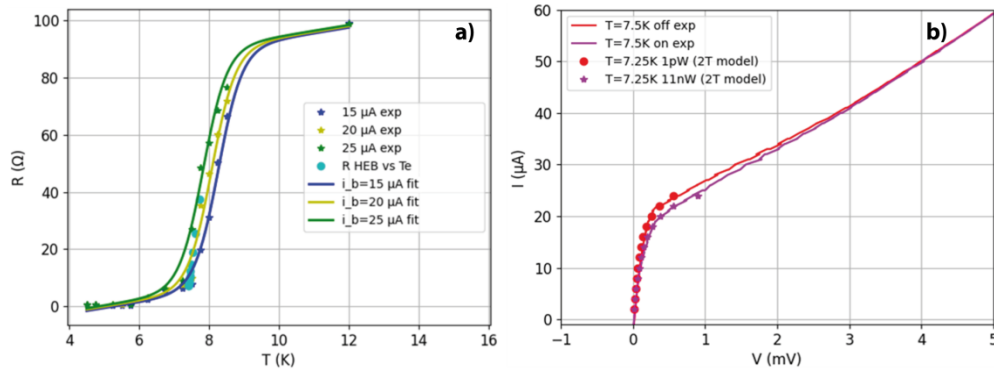


Fig. 5. (a) The intrinsic transition measured for different dc bias currents ranging between 15 and 25 μA and the modelled curve following the sigmoidal fit. We also plot (cyan dots) the resistance of the HEB (R_{HEB}) vs T_e using T_e calculated by the 2 T model at different I_b (shown in (b) as stars) and the sigmoidal fit for a power of 11 nW. (b) Experimental I-V at 7.5 K with laser off (red continuous line) and laser on (magenta, continuous line) with superposed the results of the 2 T model at $T = 7.25$ K with power $P = 1$ pW (red dots) and $P = 11$ nW (magenta stars).

The $\rho(T, I_b)$ resulting from $R(T, I_b)$ is used as HEB fingerprint in Eq. (1) (2 T model) and now using the 2 T model it is possible to predict the complete I-V characteristics. In Fig. 5(a) we also plot (cyan dots) the resistance of the HEB (R_{HEB}) vs T_e using T_e calculated by the 2 T model at different I_b (shown in b as stars) and the sigmoidal fit for a power of 11 nW. Figure 5(b) shows the experimental I-V curves at 7.5 K taken with the TDS on and TDS off. These curves are in good agreement with a set of I-V points calculated according to the 2 T model, in the limit $T_e \leq T_c(I_b)$, for a temperature $T = 7.25$ K and an impinging radiation power respectively of 1 pW and 11 nW. Starting from this result we can calculate the frequency response for different bias currents of the detector.

Figure 6 shows the simulated frequency response of the HEB at 7.25 K at two different bias points 10 and 20 μA (dotted line) showing, independently from the I_b , a 3 dB frequency cutoff ≥ 2 GHz. On the other side, the high frequency cutoff of the experimental response (continuous line) has a strong dependence from the I_b , 0.6 GHz (blue curve) and 0.15 GHz (red curve) for 10 and 20 μA , respectively. The experimental high frequency cutoff is compatible with a first-order low pass filter cutoff frequency, probably due to parasitics in the circuit (wire bonds, cryo-mount and cables) and has a strong dependence with the I_b : changing the operating point of the HEB the impedance matching is changed accordingly [17,25,26].

In addition, in the flat region (around 100 MHz) of the experimental data, we have a responsivity reduction going from 20 to 10 μA , which is in agreement with the reduction resulting from the simulation.

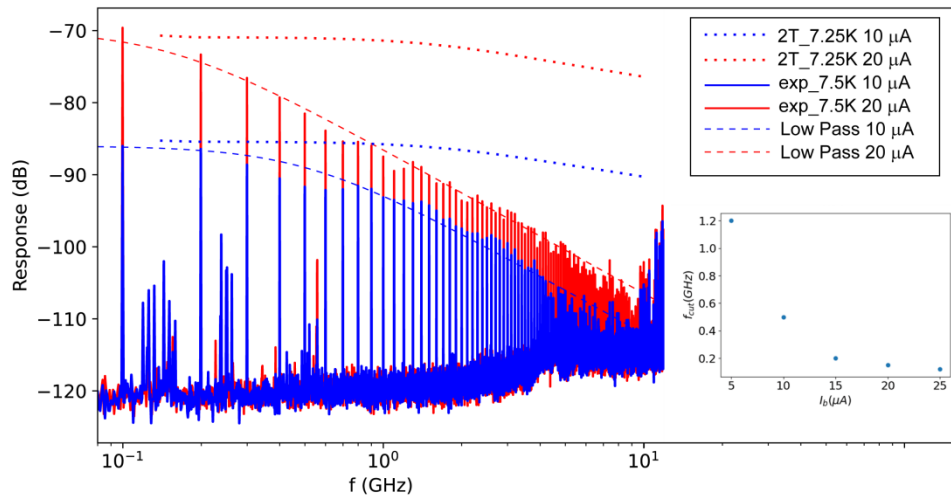


Fig. 6. Frequency response of the HEB at 7.5 K at $I_b = 10 \mu\text{A}$ (blue continuous line) and $I_b = 20 \mu\text{A}$ (red continuous line) and the result of the 2 T model at 7.25 K (dotted lines). The dashed lines show the simulated frequency response of the HEB introducing a low pass filter. Frequency cutoff vs I_b .

Furthermore Fig. 6 shows the simulated frequency response including an additional first-order low pass filter, in the two cases (dashed lines). Applying this procedure to other bias currents I_b , we obtain the result shown in Fig. 6 inset, where the corresponding cutoffs are displayed.

5. Responsivity and NEP

Important figures of merit to define HEB performances are the responsivity and its sensitivity [27], the latter characterized by the noise equivalent power (NEP), i.e., the minimum incident power required to obtain a unit signal to noise ratio in a 1 Hz bandwidth. To calibrate the HEB we used a high-power THz-QCL as input source with the active region based on four-quantum well super-diagonal structure [15] operating at 77 K mounted in a small nitrogen cryostat (about 2 dm^3 in volume). To map the intensity of the beam pattern of the QCL and perform power measurements calibration [1] for this specific QCL, we used a room temperature commercial pyro-electric detector (GENTEC model QS2-THz-BL) with an aperture diameter of 2 mm, responsivity 140 kV/W and a black HDPE window to filter the IR.

We performed a 2D map of the radiation pattern of the QCL working in pulsed mode with a duty cycle of 5%. By integrating the intensity of the beam patterns measured by the pyro-electric detector, we got an output power of about $20 \mu\text{W}$, which corresponds to a total power in continuous wave of 0.4 mW .

We now perform a new map by using the HEB and operating the QCL in the same condition. The HEB was biased at $20 \mu\text{A}$ and operated at 7.5 K. If we integrate the intensity for all pixels and take into account the cross section between the single pixel area of pyro-electric detector and the spatial resolution of the HEB, in this operating point (I_b, T) we got a responsivity of 560 V/W . We can now infer the NEP of our HEBs.

We operate the detector in direct mode setting the operating temperature with the resistive heater. The HEB can be polarized in each point of the I-V characteristics as long as dV/dI is continuous to avoid noisy instabilities in the HEB, as we said in the previous section. By changing the HEB operating point (I_b, T) the responsivity changes as well and we take this into account by

measuring the amplitude of HEB response to the QCL pulses. The detector NEP, is obtained by the ratio between the voltage noise spectral density $V_n(f)$ measured at the HEB output and the HEB responsivity. To measure the voltage noise density, we used a spectrum analyzer (FPC1500, Rohde & Schwarz) connected to the output of an amplification chain composed by the cryogenic LNA and a room temperature amplifier (SR560, Stanford Research Systems).

We point out that in these NEP measurements our setup was limited in the MHz range primarily by the limited speed of the driver modulating the QCL, required for the HEB responsivity measurements. Changing the bath temperature and the current bias we obtained a NEP below $1 \text{ pW}/\sqrt{\text{Hz}}$ biasing the device between 15 and $30 \text{ }\mu\text{A}$ at 7.5 K with a minimum NEP = $0.8 \text{ pW}/\sqrt{\text{Hz}}$.

In Fig. 7 the measured minimum NEP spectrum is shown. The $1/f$ noise at frequencies below 100 kHz is due to the cryogenic amplifier while the decrease that begins to appear at higher frequencies, is due to the room temperature amplifier which has a cutoff at 1 MHz .

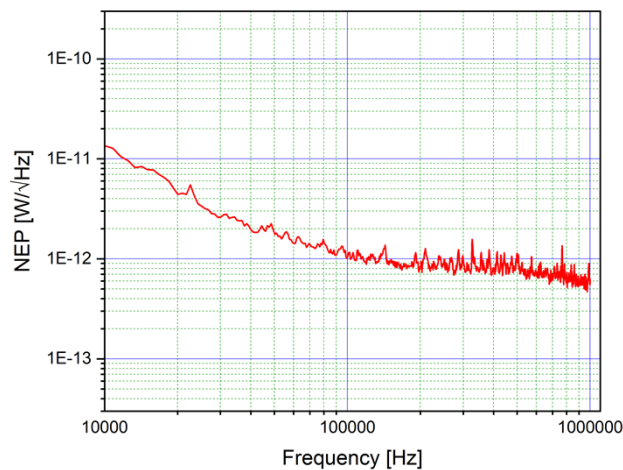


Fig. 7. Noise Equivalent Power of the HEB taken at $I_b = 20 \text{ }\mu\text{A}$ and $T = 7.5 \text{ K}$. The noise under 100 kHz is affected by the contribution of the cryogenic amplifier. The decrease that begins to appear at higher frequencies, is due to the cutoff of the room temperature amplifier.

We believe that we are underestimating the HEB sensitivity due to the direct detection effect [28], which shifts the optimal operating point to a higher voltage when using a calibration load higher than 100 nW .

We cannot provide the NEP value in the GHz band but we can estimate an upper limit in this frequency range, considering the responsivity reduction due to the attenuation that the signal has at higher frequencies (see Fig. 3(c)) and assuming, as a worst case scenario, that noise is not affected by this reduction effect and remains flat.

6. Conclusions

By using two different sources, a picosecond laser-based THz source and a THz QCL frequency comb we have shown that our phonon-cooled HEB is still highly sensitive up to 30 GHz once operated in mixer mode detecting up to the third harmonic of the beating signal of a THz QCL comb with a round trip of 10 GHz . In addition, we measured the HEB sensitivity estimating a minimum NEP of $0.8 \text{ pW}/\sqrt{\text{Hz}}$, although the direct detection effect led to underestimate the optical responsivity. We provide a full characterization of our detector in terms of frequency response, sensitivity and NEP. We show that the fabricated HEB has a 3 dB cutoff around 2 GHz at 7.5 K . According to the theoretical model we show how the frequency response of the HEB

changes, changing both the bias point and its operating temperature. Such detector has already been employed for SWIFTs characterization of THz QCL frequency combs [29]

Our next challenge is to optimize the HEB technology in terms of the rf coupling (coplanar waveguide design on chip as well as the rf packaging on the rf connector) but also from the bolometer technology point of view, i.e., improving the quality of the contact pads interface itself: all ingredients needed for targeting a higher frequency cutoff limit [12,17,30]. This high-speed and high-sensitivity detector can find several applications in combination with THz frequency combs for the diagnostic of the comb itself but also in the field of atomic and molecular broadband spectroscopy [31].

Funding. Horizon 2020 Framework Programme (Actphast4R, P2020-41).

Acknowledgments. S.C. and G.S. would like to thank Juraj Darmo for helpful discussion.

Disclosures. The authors declare no conflicts of interest

Data availability. Data underlying the results presented in this paper are not publicly available at this time but may be obtained from the authors upon reasonable request.

Supplemental document. See [Supplement 1](#) for supporting content.

References

1. B. Mirzaei, J. R. G. Silva, D. Hayton, C. Groppi, T. Y. Kao, Q. Hu, J. L. Reno, and J. R. Gao, "8-beam local oscillator array at 4.7 THz generated by a phase grating and a quantum cascade laser," *Opt. Express* **25**(24), 29587–29596 (2017).
2. L. Viti, D. G. Purdie, A. Lombardo, A. C. Ferrari, and M. S. Vitiello, "HBN-encapsulated, graphene-based, room-temperature terahertz receivers, with high speed and low noise," *Nano Lett.* **20**(5), 3169–3177 (2020).
3. D. Dietze, J. Darmo, and K. Unterrainer, "Efficient population in modulation doped single quantum wells by intense few-cycle terahertz pulses," *New J. Phys.* **15**(6), 065014 (2013).
4. D. Burghoff, T. Yu-Kao, N. Han, C. W. I. Chan, X. Cai, Y. Yang, D. J. Hayton, J. R. Gao, and Q. Hu, "Terahertz laser frequency comb," *Nat. Photonics* **8**(6), 462–467 (2014).
5. J. Faist, G. Villares, G. Scalari, M. Rösch, C. Bonzon, A. Hugi, and M. Beck, "Quantum Cascade Laser Frequency Combs," *Nanophotonics* **5**(2), 272–291 (2016).
6. A. Forrer, S. Cibella, U. Senica, G. Torrioli, M. Beck, J. Faist, and G. Scalari, "Shifted Wave Interference Fourier Transform Spectroscopy of Harmonic and Fundamental RF Injection-Locked THz Quantum Cascade Laser Frequency Combs," *27th International Semiconductor Laser Conference* (2021), pp. 1–2.
7. A. Baryshev, J. N. Hovenier, A. J. L. Adam, I. Kašalynas, and J. R. Gao, "Phase locking and spectral linewidth of a two-mode terahertz quantum cascade laser," *Appl. Phys. Lett.* **89**(3), 031115 (2006).
8. E. Brundermann, H.-W. Hubers, and M. F. Kimmittin, *Terahertz Techniques* (Springer Series in Optical Sciences, 2012).
9. A. Shurakov, Y. Lobanov, and G. Goltsman, "Superconducting hot-electron bolometer: from the discovery of hot-electron phenomena to practical applications," *Supercond. Sci. Technol.* **29**(2), 023001 (2016).
10. F. Martini, S. Cibella, A. Gaggero, F. Mattioli, and R. Leoni, "Waveguide integrated hot electron bolometer for classical and quantum photonics," *Opt. Express* **29**(6), 7956–7965 (2021).
11. T. M. Klapwijk and A. V. Semenov, "Engineering Physics of Superconducting Hot-Electron bolometer mixer," *IEEE Trans. Terahertz Sci. Technol.* **7**(6), 627–648 (2017).
12. S. A. Ryabchun, I. V. Tretyakov, M. I. Finkel, S. N. Maslennikov, N. S. Kaurova, V. A. Seleznev, B. M. Voronov, and G. N. Goltsman, "Fabrication and characterisation of NbN HEB mixers with in situ gold contacts," *19th International Symposium on Space Terahertz Technology* (2008).
13. S. Cibella, M. Ortolani, R. Leoni, G. Torrioli, L. Mahler, J. H. Xu, A. Tredicucci, H. E. Beere, and D. A. Ritchie, "Wide dynamic range terahertz detector pixel for active spectroscopic imaging with quantum cascade lasers," *Appl. Phys. Lett.* **95**(21), 213501 (2009).
14. J. Hillbrand, L. M. Krüger, S. Dal Cin, H. Knötig, J. Heidrich, A. M. Andrews, G. Strasser, U. Keller, and B. Shawar, "High-speed quantum cascade detector characterized with a mid-infrared femtosecond oscillator," *Opt. Express* **29**(4), 5774–5781 (2021).
15. A. Forrer, M. Franckić, D. Stark, T. Olariu, M. Beck, J. Faist, and G. Scalari, "Photon-Driven Broadband Emission and Frequency Comb RF Injection Locking in THz Quantum Cascade Lasers," *ACS Photonics* **7**(3), 784–791 (2020).
16. Y. Zhuang and K. S. Yngvesson, "Negative Resistance Effects in NbN HEB Devices," *12th Intern. Symp. Space THz Technol.* (2001), pp. 143–153.
17. A. D. Semenov and H. W. Hübers, "Bandwidth of a Hot-Electron Bolometer Mixer According to the Hotspot Model," *IEEE Trans. Appl. Supercond.* **11**(1), 196–199 (2001).
18. A. D. Semenov, G. N. Gol'tsman, and R. Sobolewski, "Hot-electron effect in superconductors and its applications for radiation sensors," *Supercond. Sci. Technol.* **15**(4), R1–R16 (2002).

19. A. D. Semenov, R. S. Nebosis, Y. P. Gousev, M. A. Heusinger, and K. F. Renk, "Analysis of the nonequilibrium photoresponse of superconducting films to pulsed radiation by use of a two-temperature model," *Phys. Rev. B* **52**(1), 581–590 (1995).
20. R. Barends, M. Hajenius, J. R. Gao and, and T. M. Klapwijk, "Current-induced vortex unbinding in bolometer mixers," *Appl. Phys. Lett.* **87**(26), 263506 (2005).
21. M. Hajenius, R. Barends, J. R. Gao, T. M. Klapwijk, J. J. A. Baselmans, A. Baryshev, B. Voronov, and G. Gol'tsman, "Local Resistivity and the Current-Voltage Characteristics of Hot Electron Bolometer Mixers," *IEEE Trans. Appl. Supercond.* **15**(2), 495–498 (2005).
22. I. Tretyakov, S. Ryabchun, M. Finkel, A. Maslennikova, N. Kaurova, A. Lobastova, B. Voronov, and G. Gol'tsman, "Low noise and wide bandwidth of NbN hot-electron bolometer mixers," *Appl. Phys. Lett.* **98**(3), 033507 (2011).
23. E. M. Gershenson, M. E. Gershenson, G. N. Goltsman, A. Lul'kin, A. Semenov, and A. Sergeev, "On the limiting characteristics of high-speed superconducting bolometers," *J. Techn. Phys.* **59**(2), 111–120 (1989).
24. R. Barends, M. Hajenius, J. Gao, and T. Klapwijk, "Direct correspondence between HEB current-voltage characteristics and the current-dependent resistive transition," *16th International Symposium on Space Terahertz Technology* (2005).
25. B. S. Karasik and W. R. McGrath, "Microwave transmission technique for accurate impedance characterization of Superconductive Bolometric Mixers," *Int. J. Infrared and Millimetre Waves* **20**(1), 21–32 (1999).
26. E. M. Gershenson, G. N. Gol'tsman, I. G. Gogidze, Y. P. Gusev, A. I. Elant'ev, B. S. Karasik, and A. D. Semenov, "Millimeter and submillimeter range mixer based on electron heating of superconducting films in the resistive state," *Superconductivity* **3**, 1582 (1990).
27. S. Seliverstov, S. Maslennikov, S. Ryabchun, M. Finkel, T. M. Klapwijk, N. Kaurova, Y. Vachtomin, K. Smirnov, B. Voronov, and G. Goltsman, "Fast and sensitive Terahertz direct detector based on superconducting antenna-coupled hot electron bolometer," *IEEE Trans. Appl. Supercond.* **25**(3), 1 (2014).
28. J. J. A. Baselmans, A. Baryshev, S. F. Reker, M. Hajenius, J. R. Gao, T. M. Klapwijk, Y. Vachtomin, S. Maslennikov, S. Antipov, B. Voronov, and G. Gol'tsman, "Direct detection effect in small volume hot electron bolometer mixers," *Appl. Phys. Lett.* **86**(16), 163503 (2005).
29. U. Senica, A. Forrer, T. Olariu, P. Micheletti, S. Cibella, G. Torrioli, M. Beck, J. Faist, and G. Scalari, "Planarized THz quantum cascade lasers for broadband coherent photonics," *Light: Sci. Appl.* **11**(1), 347 (2022).
30. J. J. A. Baselmans, M. Hajenius, J. R. Gao, A. Baryshev, J. Kooi, T. M. Klapwijk, B. Voronov, P. de Korte, and G. Gol'tsman, "NbN hot electron bolometer mixers: sensitivity, LO power, direct detection and stability," *IEEE Trans. Appl. Supercond.* **15**(2), 484–489 (2005).
31. T. Hearne, M. H. Mammez, D. Mammez, M. A. Martin-Drumel, P. Roy, O. Pirali, S. Eliet, S. Barbieri, F. Hindle, G. Mouret, and J. F. Lampin, "Unlocking synchrotron sources for TH spectroscopy at sub-MHz resolution," *Opt. Express* **30**(5), 7372 (2022).